Signatures of clustering accessible with a Time Projection Chamber: TexAT

Jack Bishop[1,2,*], *S.* Ahn[2,5], *M.* Barbui[2], *Tz.* Kokalova[1], *E.* Koshchiy[2], *C.E.* Parker[2,6], *S.H.* Pirrie[1], *E.C.* Pollacco[7], *B.T.* Roeder[2], *G.V.* Rogachev[2,3,4], *A.* Saastamoinen[2], and *C.* Wheldon[1]

[1]School of Physics and Astronomy, University of Birmingham, Edgbaston, Birmingham, B15 2TT, United Kingdom
[2]Cyclotron Institute, Texas A&M University, College Station, TX 77843, USA
[3]Department of Physics & Astronomy, Texas A&M University, College Station, TX 77843, USA
[4]Nuclear Solutions Institute, Texas A&M University, College Station, TX 77843, USA
[5]Center for Exotic Nuclear Studies, Institute for Basic Science, 34126 Daejeon, Republic of Korea
[6]Department of Physics and Astronomy, Ohio University, Athens, OH 45701, USA
[7]IRFU, CEA, Université Paris-Saclay, Gif-Sur-Yvette, France

Abstract. Many experimental observables in clustering require high-sensitivity, almost background-free measurements. The use of Time Projection Chambers (TPCs) over the past 15 years have demonstrated their capability as a step change in the accessibility of many of these observables, as well as the possibility to study clustering via new techniques.
A summary of the difficulties and pitfalls of determining the type of clustering from observables is briefly discussed, with a focus on α-condensation and the possibility of an additional (Efimov) 0^+ state in ^{12}C, below the Hoyle state. The expansion of the technique used to tackle this challenge to study $3\alpha + p$ clustering in ^{13}N is also discussed, highlighting the exciting opportunities TPCs provide to study clustering inaccessible by conventional means.
Finally, an overview of the recent and upcoming advances in TPC technology is given as well as listing additional future challenges that are needed to be overcome, in the context of discussing the next-generation upgrade to the existing TexAT TPC, known as TeBAT (TExas Birmingham Active Target).

1 Introduction

When studying exotic signatures of α-clustering, in particular clustering such as condensation [1] and linear-chain configurations [2], the experimental observables may require high sensitivity in order to separate the more conventional cluster configurations. It is important to develop a clear and fair null hypothesis that 'this signature can be described by conventional α-clustering rather than the exotic form of α-clustering' which one can then reject with a high precision measurement of an experimental observable in comparison to two theoretically-robust (or with well-quantified errors) predictions for the different scenarios. If a given experimental observable is consistent with both a normally-clustered α-particle state and an α-condensate for example, we cannot take this observable as **evidence** of α-condensation as has been claimed in some experiments — it is merely consistent with it. This in fact is a logical fallacy known as the 'fallacy of affirming the consequent' [3] and also 'underdetermination'. Consequently, future experiments should choose an alternate observable to differentiate these hypotheses. In reality, these different observables may be even harder to measure or have an absence of theoretical predictions but, to make a definitive statement about the existence/non-existence of these states, an alternative route is necessary.

In order to statistically meaningfully reject the null hypothesis for situations where the observable is a small branching ratio, minimising the background is paramount. One experimental detector system that is becoming increasingly popular and powerful at addressing this challenge is the Time Projection Chamber (TPC).

2 Time Projection Chambers

TPCs comprise a vacuum vessel that is filled with a gas (with specific restrictions, discussed below). Surrounding the gas volume, a field cage is constructed which, via a series of high voltage wires progressively stepping down in voltage, produces a linear electric field known as the drift field. As charged particles pass through the gas volume, they undergo energy loss and produce electrons and ions from the gas. The drift field separates the two opposing charges and the electrons are drifted onto a position-sensitive readout system to measure the incident charge. The position sensitivity in combination with the arrival time of the drifted electrons allows for a full 3D reconstruction of the charged-particle tracks in the gas volume — see Fig. 1. The primary electrons drifted through the gas volume are however insufficient to be readout via charge-sensitive amplifiers and as such are amplified by a strong electric field (> 1 kV/mm) immediately above the

*e-mail: j.bishop.2@bham.ac.uk

position-sensitive readout over the distance of a few hundred microns which causes a Townsend avalanche and a very large associated gas gain. The most commonly used device for this is known as a Micromegas (Micro-Mesh Gaseous Structure) [4].

When operating in 'active-target mode', the gas used inside of the TPC is simultaneously the readout medium and also the target. This is an extremely powerful mode of operation as the effective target thickness versus a solid target can be an order of magnitude or more higher without the associated energy straggling issues as the interaction vertex can be identified and the correct energy loss correction made. Not all gases are suited for readout in a TPC however. Their ionisation properties may cause breakdown in the Micromegas due to the production of UV photons during the avalanche process that can induce a secondary avalanche process non-locally. If this process continues, the Micromegas will spark and damage may occur. For some undesirable gases (such as helium) for which this occurs, a small amount of a quenching gas which reduces the secondary avalanche process is added (typically CO_2) at a few percent level. New innovative Micromegas designs physically prevent this secondary avalanche process and, as such, can run with pure helium gas [5].

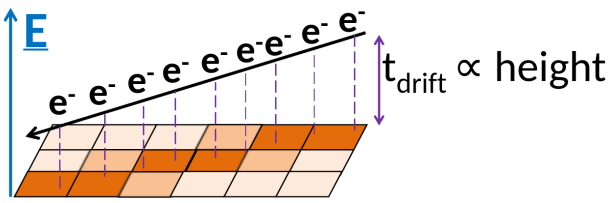

Figure 1. Schematic demonstrating how the combination of position information (denoted by the strength of colours on the pixels shown) with the drift time (denoted by the dashed lines) allows for the full 3D track to be reconstructed. Random scattering processes in the gas also causes a dispersion of the drift electrons in the transverse and longitudinal direction that can be potentially beneficial to get sub-pixel resolution via fitting the charge spread across multiple pixels.

Due to the fact that all charged-particles within the gas volume are observed with an exceptionally-low energy threshold, the use of TPCs allows for a high-sensitivity, low-background approach to the measurement of many signatures of α-clustering in light nuclei. This work will focus on experiments performed with the TexAT (TEXas Active Target) TPC.

3 TexAT

TexAT [6] is a rectilinear TPC with an active area of 224 x 245 x 130 mm^3 in the beam, perpendicular and drift directions respectively — the CAD is shown in Fig. 2. The position sensitive readout is a 128-μm-high Micromegas detector with pads of 1.75 x 3.5 mm in the central beam region (8 pads wide) with the side regions being multiplexed into strips and chains to reduce the number of electronics channels. The pads are read out via the General Electronics for TPCs (GET) system which is widely used across nuclear physics TPCs and fully digitises the waveforms with a clock speed of up to 100 MHz with 12-bit ADCs for 512 time buckets. Collections of 64 channels are fed into an AGET chip with a single ASIC-ADC (AsAd) board containing 4 ASIC for GET (AGET) chips. Then, 4 AsAd boards are then read out by a Concentration Board (CoBo) which sits in a μTCA crate from where the data are sent over Ethernet to the data acquisition machine. Each CoBo therefore can read out 1024 channels. For the TexAT electronics setup, the triggering and timing is controlled by a μTCA Multiplicity Timing And Triggering (MuTAnT) module.

Since commissioning in 2017, TexAT has been used to study a variety of exotic clustering signatures with a multitude of techniques.

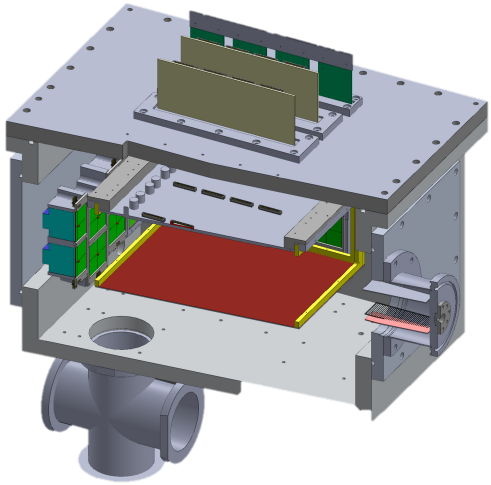

Figure 2. CAD of the TexAT Time Projection Chamber. The gas is contained within a 1-inch-thick aluminium chamber with the beam entering through a 4-μm-thick Havar window at the right. The active area of the TPC is denoted by the space occupied by the red (online) rectangle which is the negatively-charged cathode which defines the start of the drift field. The Micromegas sits at the top of the chamber (shown dissected) where the positive field is applied that attracts drift electrons. The TPC can also be surrounded by an array of silicon detectors backed by caesium-iodide detectors that measure the energy of particles that escape the active region.

4 Signatures of α-condensates

The archetypal case of α-clustering is that of the Hoyle state in ^{12}C, sitting above the 3α-decay threshold with an excitation energy of 7.65 MeV. The specific form of clustering, whether a bent-arm configuration [7], a triangular arrangement [8], a linear chain configuration [2] (disproven by the rotational band's moment of inertia) or a dilute gas of α-particles known as an α-condensate [1], has been a question since the existence of the state was experimentally confirmed [9]. The last of these postulated structures has received renewed interest in the past 25 years

with the advent of the THSR wavefunction [1] which is a physically-motivated wavefunction ansatz that treats the α particles in a condensate as a weakly-interacting pseudoboson gas. The question of what specific observables would characterise a state as an α-condensate is a difficult one that was tackled a few years after the THSR wavefunction [10]. Since then, the experimental community has focused on a specific observable — the observation of the direct decay of the Hoyle state, not through the intermediate ^{8}Be system but directly into three α particles. For an α-condensate, this direct decay component is expected to be enhanced relative to a traditionally α-clustered state (due to the similarity in their wavefunctions). Theoretical predictions of the exact value for the two scenarios have been difficult to calculate due to the dependence of the three-body breakup model chosen and the influence of the ghost for the ^{8}Be ground state [11, 12].

Experimentally, a series of measurements [13–17] followed an anomalous measurement [18] which converged on an upper limit at the 95% confidence level to a direct decay branching ratio of $< 0.02\%$. Theoretical predictions for the α-condensate lay around the 0.01% value so a large improvement in experimental technique was necessary to be able to measure an absolute branching ratio rather than a limit.

To overcome the fundamental limitations of silicon detector approaches to measure the direct decay (mainly random coincidences), the TexAT TPC was used to study the decay of the Hoyle state at rest by populating the state via β-decay of ^{12}N [19]. By implanting and stopping the ^{12}N inside the gas, the β energy loss is sufficiently small to not contribute to the tracks of the 3 α particles that can have their energy and momentum reconstructed. To ensure the measurement remains background free, the ^{12}N is implanted one ion at a time and only once it has had sufficient time to decay, is a new ion implanted. To measure the direct decay component, two metrics were used to separate the sequential decay component: the angle between the 3 α-particles and the energy partition (where direct decays have a preference for an equal energy sharing rather than one α-particle taking $\approx 50\%$ of the decay energy). Examples of both of these events are demonstrated in Fig. 3. A Bayesian approach was used to determine the likelihood distribution of the direct decay branching ratio based on an ensemble of 19,000 decays which were assigned a probability of being either direct or sequential, event-by-event. The results of this work are shown in Fig. 4 where for the first time, sensitivity to the absolute branching ratio was demonstrated rather than an upper limit. The most likely branching ratio is 0.01%, entirely commensurate with the upper limits seen by previous measurements.

This result was then used to examine our null hypothesis that these data are consistent with a traditionally α-clustered state rather than an α-condensate. There was first one additional complication, what we observed in our experiment are what we describe as "direct-like" decays rather than direct decays. This is due to the possibility that the Hoyle state is decaying through the ghost of the ^{8}Be(g.s). The strength of this contribution can be as large as 0.01%, i.e. the branching ratio we observed. Disentangling the direct-like from the true direct decays is therefore extremely difficult and the baton of understanding is then passed towards further theoretical studies. A robust estimation of the strength of decays through the ghost would then mean the remaining strength would be attributed to true direct decays. Current predictions (with large error bars due to different models) pin the ghost contribution to around 0.01% (but also at large as 0.06% [12]) suggesting the true direct component is much smaller — in agreement with a separate indirect measurement [20] with an optical TPC (which relied on assumptions about the Hoyle state rotational band).

Returning to the hypotheses, we are obviously unable to state that the branching ratio observed is inconsistent with a geometric α-clustered state (i.e. the null hypothesis cannot be rejected). Additionally, we are also unable to unequivocally state our data are inconsistent with an α-condensate without additional theoretical input.

This specific case highlights not only the unparalleled sensitivity of TPCs to achieve measurements that are just beyond the limits of even the best-designed silicon detector array experiments, but also the care one must take when evaluating the agreement between theoretical models and experimental data. The agreement of our observations with hypothesis A (that the Hoyle state is an α-condensate) does not mean hypothesis A is true if it is also in agreement with hypothesis B (that the Hoyle state is a geometrically α-clustered state) if A and B are mutually exclusive hypotheses.

5 3α Efimov states

A related scenario has also been addressed with the claimed observation of anomalous signatures in heavy ion collisions where structure is seen in ^{12}C at an energy of 7.458 MeV. This state has varyingly been ascribed as a possible Efimov state or a Thomas state [21–23] as a manifestation of the general quantum phenomenon where a three-body system can become more bound due to the interplay of the unbound two-body subsystems creating a system with a large radius than exceeds the two-body force range. Using the same dataset as the experiment above, stringent limits were placed based on the population of such a state via the β-decay of ^{12}N multiplied by the α-decay branching ratio [24], shown in Fig. 5, which was possible due to the extremely-low energy threshold inside the TPC of 10 keV (without a contribution from the β particle). Utilising previous data from Gammasphere which examined the β-decay of ^{12}B (which will contain the same population strength information) [25], stringent limits were also placed on the non-observation in the γ-decay channel. Additionally, an astrophysical argument was also made where if such a state were to α-decay sequentially rather directly, it would be inconsistent with the red giant phase of stars.

Subsequent work by another group took data obtained with the CHIMERA detector at INFN LNS which were examined to look for the same signature in the α-decay channel [26]. They examined the expected contribution of an Efimov state to their expected excitation function from

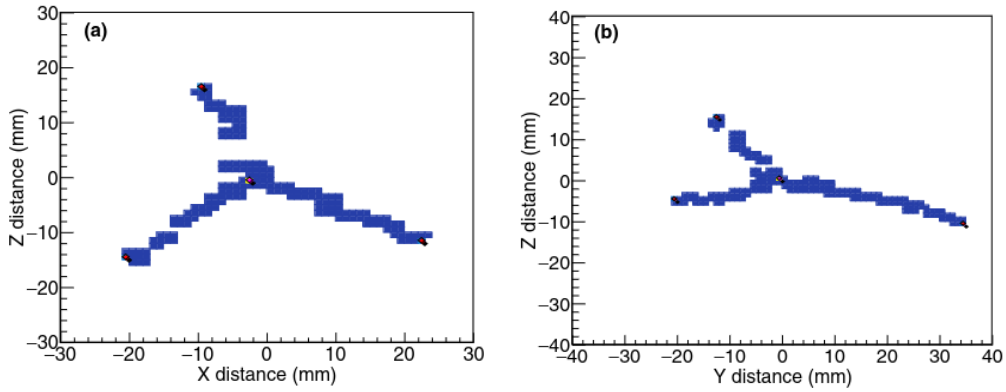

Figure 3. 2D projections of 3D TexAT tracks. a) An example of a direct-like Hoyle state decay showing a more equal energy sharing of the 3 α-particles. b) An example of the 'Y' shape corresponding to sequential decay through the ^{8}Be ground state. Measuring the full tracks of all charged-particles provides the sensitivity to observe the very rare direct-like decay for the first time with confidence the event does not originate from pile-up. As shown in Ref. [19].

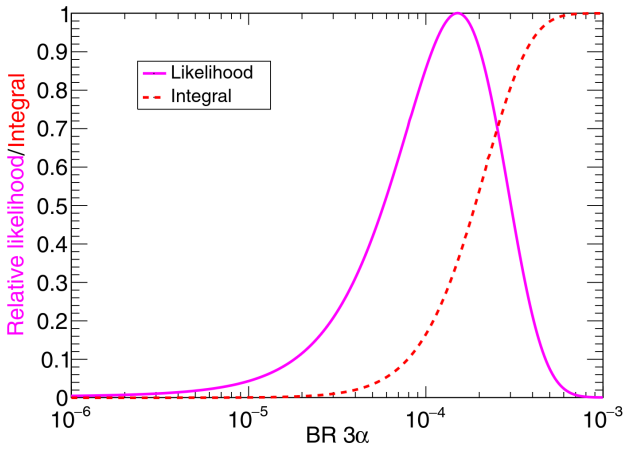

Figure 4. The solid magenta line shows the likelihood distribution for the direct decay branching ratio from the TexAT data set. The most likely value is 10^{-4}, i.e. 0.01%. One can also obtain a 95% confidence level limit from the data of 0.043% which agrees with existing data. One can also determine that the direct 3α branching ratio is $>10^{-5}$ at the 95% confidence level due to the observation of several 'direct-like' events. As shown in Ref. [19].

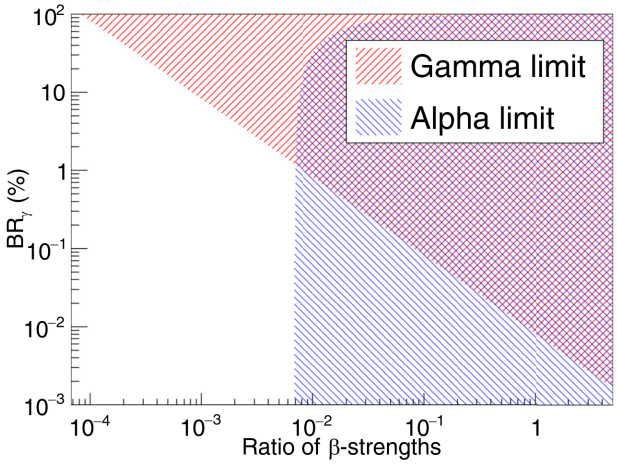

Figure 5. The 95% confidence level exclusion plot for the non-observation of an Efimov state from the TexAT data with varying β-decay population strengths (relative to the Hoyle state) against different γ-decay branching ratios. Our data are inconsistent with the observation of an Efimov state unless the state is populated at a level of $< 1\%$ that of the Hoyle state for all branching ratio values. As shown in Ref. [24].

^{12}C(α, α'). The conclusion of this work was that they were able to exclude the presence of a state if it were to undergo sequential decay, but their data are 'compatible with its direct decay' despite the sequential decay expected to dominate. While their conclusions acknowledge the possibility that this state does not exist, one must be careful to frame the conclusions of this work properly else generate another case of 'fallacy of affirming the consequent': if a direct-decaying Efimov state were to exist, it would be consistent with their current data but the fact that their data are consistent with that hypothesis does not mean one can infer a direct-decaying Efimov state exists. This highlights the difficulty in rejecting the null hypothesis when the experimental set-up does not have the sensitivity required due to the background limitations of large silicon detector arrays. While a solely direct-decaying Efimov state would be consistent with the astrophysical argument made in our previous work [24] which assumed a sequential decay mode, this is still inconsistent with our TexAT result as well as many high-resolution inelastic scattering measurements that will be published shortly (where the missing mass technique is agnostic of the decay mechanism which should be γ-decay dominated).

6 Cluster physics via new decay modes

The experimental method of β-delayed charged-particle spectroscopy was shown by the work highlighted in the previous two sections to be a very powerful tool for work in the high-sensitivity regime for studying previously-known resonances in ^{12}C. Adding just one proton to the ^{12}C system to make ^{13}N affords a fantastic opportunity to understand how clustering evolves from α-conjugate to molecular cluster systems. The most commonly used approach to study α-clustering in a new system is the use of Thick Target in Inverse Kinematics (TTIK) to study the α-particle elastic scattering cross section at large angles, away from the Rutherford regime [27]. For ^{13}N, this necessitates the study of ^{9}B(α,α). Unfortunately nature does not make life so simple for experimentalists, ^{9}B is unstable and with a lifetime of 0.54 keV (10^{-18} s), not even in-flight radioactive beams techniques will allow for a measurement of this reaction. Additionally, even if we are able to populate these α-clustered states in ^{13}N by other means, these states will decay into 3α+p (either through $\alpha+^{9}B \rightarrow \alpha + (^{8}\mathrm{Be} + p) \rightarrow \alpha + (\alpha + \alpha + p)$ or $p + ^{12}\mathrm{C}(0^{+}_{2}) + p \rightarrow (^{8}\mathrm{Be} + \alpha) + p \rightarrow (\alpha + \alpha + \alpha) + p)$). One therefore needs to measure these four particles and then use invariant mass reconstruction to obtain the excitation energy and decay channels. To obtain reasonable statistics with a silicon detector array, one needs both a very high solid angle coverage and high beam current making the probability of pile-up/event mixing very high and therefore the excitation energy spectrum will likely have a very large background.

Instead, we populated ^{13}N via the β-decay of ^{13}O and implanted the ^{13}O into the TexAT TPC as achieved previously with the ^{12}N beam. Observing the four particles after one-at-a-time implant and decay inside the TPC naturally comes with a 100% solid angle coverage and an almost background-free measurements can be made.

Our experimental set-up for this work [28, 29] was extremely similar to the previous experiment [19] but with a higher gas pressure of 50 Torr of CO_2. A beam of ^{13}O with an energy of 15.1 MeV/u and an intensity of 5 pps was produced via the ^{3}He(^{14}N, ^{13}O) with the K500 Cyclotron and Momentum Achromat Recoil Separator (MARS) at the Texas A&M University Cyclotron Institute. A total of 1.9 $\times 10^{5}$ ^{13}O ions were implanted and events were selected where states above the α-particle decay threshold in ^{13}N were populated that decayed into 3α+p. In total, 149 such β-delayed 3αp events were observed giving a branching ratio of 0.078(6)% and this rare decay mode was observed for the first time.

Due to the finite stopping power afforded by the size of our TPC and the chosen gas pressure, only 102 of the 149 events were available to be fully reconstructed due to high energy α-particles exiting the active region of the TPC. For almost all events, the proton had sufficient range to exit the active area, however, the proton was reconstructed from momentum conservation by measuring the momentum vectors of the α-particles from their range in the gas. With the information on the four particles, the invariant masses for ^{8}Be, ^{9}B, ^{12}C and ^{13}N could be ascertained. The

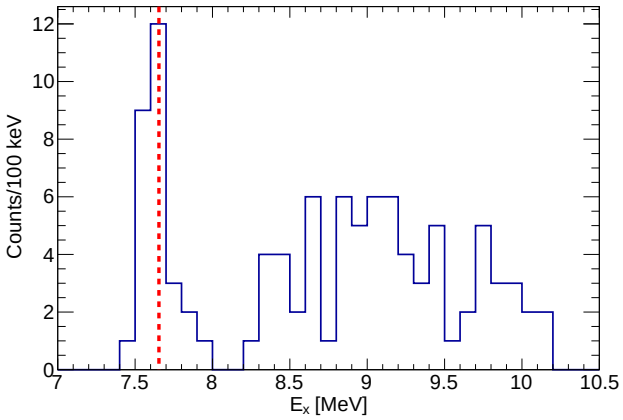

Figure 6. Invariant mass excitation spectrum for β-delayed 3αp events. The expected energy of the Hoyle state at 7.654 MeV is shown by a dashed red vertical line. For energies above E_x = 8 MeV, these events were reconstructed to test for states in ^{9}B. As shown in Ref. [29].

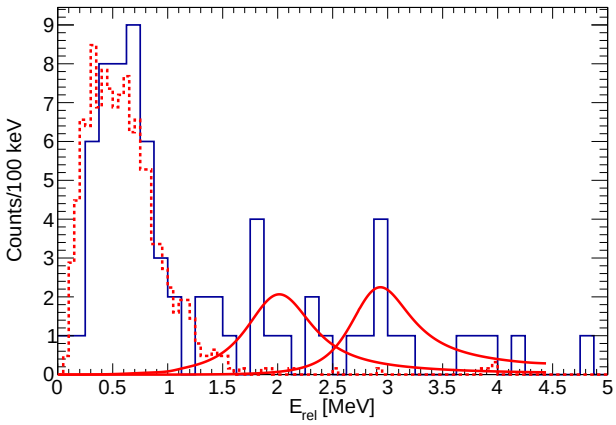

Figure 7. Relative energy spectrum for ^{9}B from ^{8}Be(g.s)+p. The dashed red line shows the GEANT4 simulation contribution expected for the ground state which replicates the data well. The expected lineshapes for the $J^{\pi} = \frac{1}{2}^{+}$ and $\frac{5}{2}^{+}$ resonances are shown by a solid red line. As shown in Ref. [29].

first step was to take the lowest-energy pairs of α-particles to ensure that decays proceeded through the ^{8}Be ground state. All except 2 events had a relative energy commensurate with the 92 keV ground state for ^{8}Be. With the two α-particles that originated from ^{8}Be identified, both the ^{9}B and ^{12}C invariant mass spectra were produced to identify whether the states in ^{13}N first underwent α-particle decay or proton decay. The excitation spectrum for ^{12}C is shown in Fig. 6 where a strong peak corresponding to the Hoyle state can be seen with a broad continuum at higher energies. A gate was placed around the 7.65 MeV peak with these states identified as having a p_2 decay channel and the relative energy spectrum for ^{9}B was measured for events with ^{12}C(E_x) > 8 MeV. The ^{9}B relative energy spectrum, shown in Fig. 7, then showed evidence of three states in ^{9}B that were populated from the α decay of ^{13}N. The ground state (expected at 278 keV) has an unusual shape (due to

the propagation of errors in the proton momentum due to uncertainties in the α-particle energy-range relation at low energies) which was well-replicated by GEANT4 simulations shown by the dashed red line. Additionally, yield can be seen above the ground state contribution with strength around 2 and 3 MeV. These were identified, as shown by the solid red lines in the figure, as originating from the $\frac{1}{2}^+$ and $\frac{5}{2}^+$ states in ^{9}B. While statistics are poor for the $\frac{1}{2}^+$, it was impossible to replicate the data without it and the parameters are consistent with the work of Wheldon et al. [30]. The exact parameters of this state are still much discussed as two possible excitation energies have been proposed, one at $E_x \approx 0.8$ MeV and one at $E_x \approx 1.8$ MeV with much ongoing experimental work attempted to rectify this disparity. Population of this state is extremely difficult however and the current work highlights that population via ^{13}N* may prove a viable production route. As discussed above, the difficulty of measuring 4 particles with high resolution is extremely difficult however and resonantly populating ^{13}N via ^{12}C(p,α) as suggested by Fortune and Sherr [31] means that the α-particles will lose a lot of energy inside the target and may not be detectable and missing mass may be required, significantly increasing the background. Subsequently, measurement of the ^{9}B($\frac{1}{2}^+$) via β-delayed charged-particle spectroscopy with a TPC, optimised for the energy of the α-particles originating from the reaction provides the best current opportunity to rectify this long-standing issue of the position of the ^{9}B($\frac{1}{2}^+$) state with a well-understood mirror in ^{9}Be. The Thomas-Ehrmann for this mirror system then affords the opportunity to study one of the simplest molecular configurations. Unfortunately, the limitation of the β-decay population rules means that one cannot study ^{9}B($\frac{1}{2}^+$) from ^{9}C decay due to its $J^\pi = \frac{3}{2}^-$ ground state meaning the population of negative parity states ($J^\pi = \frac{1}{2}^-$, $\frac{3}{2}^-$ and $\frac{5}{2}^-$) in ^{9}B will dominate.

By identifying the decay channel for the states in ^{13}N as being p_2, α_0, α_1 or α_3, the ^{13}N excitation energy spectrum was generated for the four channels. This is shown in Fig. 8 where a series of four new states were observed. After correcting for the efficiency to reconstruct different reaction channels (i.e. where α particles may escape the active area) as a function of excitation energy, the branching ratio for these states was determined. While we lacked the resolution to determine the total width of these states, the ratio to the Wigner limit could not be determined to examine the magnitude of clustering, we were able to identify the dominant form of clustering. These four states were seen to have a [^{9}B(g.s) $\bigotimes \alpha$/ ^{12}C(0_2^+) + p], [^{9}B($\frac{1}{2}^+$) $\bigotimes \alpha$], [^{9}B($\frac{5}{2}^+$) $\bigotimes \alpha$] and [^{9}B($\frac{5}{2}^+$) $\bigotimes \alpha$] structure showing the evolution of clustering to be strong when adding valence nucleons onto ^{12}C. Preliminary results on the mirror system of ^{14}O:^{14}C studying the next step of this clustering evolution with TexAT via ^{10}C(α, α), presented as part of the conference, will be submitted shortly.

This experiment on ^{13}N neatly demonstrates the power to measure clustering with a TPC from a beam intensity of only 5 pps. A very small $\beta 3\alpha$p branching ratio of 0.078% was obtained and the ability to disentangle the decay products meant that structural information about ^{13}N, inaccessible by TTIK, was determined showing the prevalence of both [^{9}B $\bigotimes \alpha$ and p + ^{12}C(0_2^+)] clustering. Overcoming limitations in terms of the resolution to which one can reconstruct the momentum vectors of the particles would provide even greater insight into this system. The next generation of TPCs may offer such opportunities.

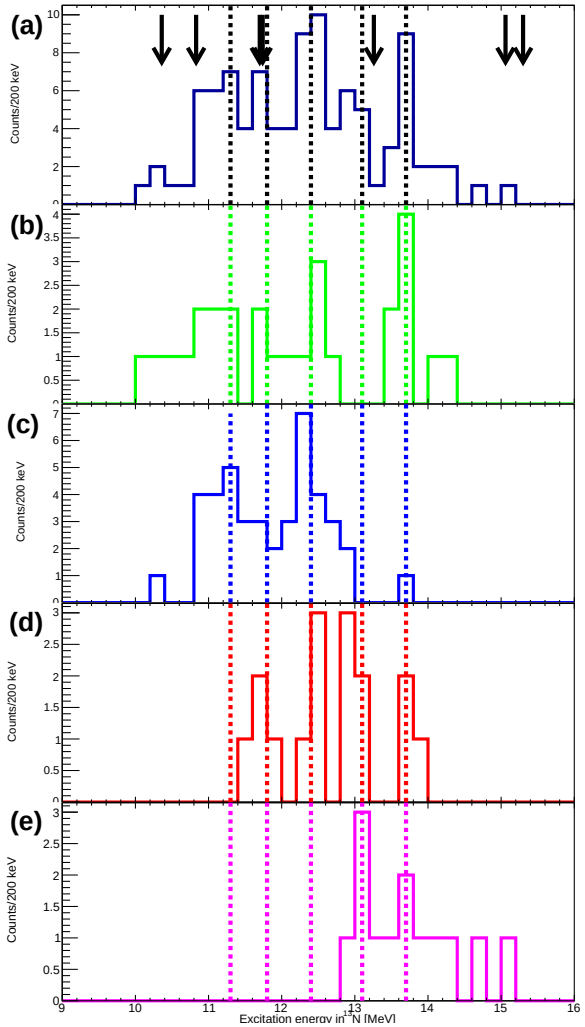

Figure 8. Excitation spectrum in ^{13}N for $3\alpha + p$ separated by decay channels: a) The sum of all channels, b) p_2, c) α_0, d) α_1, and e) α_3. The locations of previously-observed states are shown at the top by black arrows [32] with the observed states in the current work shown by vertical dashed lines. As shown in Ref. [29].

7 Next generation of TPCs

In order to better access increasingly-difficult-to-measure experimental signatures — detector advances are required and there have recently been a number in the areas of Time Projection Chambers. These will be briefly discussed and how they can improve the quality of our data to access α-clustering signatures, examined through a lens of ongoing design and construction for the TeBAT (TExas Birmingham Active Target) TPC, the next-generation upgrade to TexAT.

7.1 Pure gases and higher pressures

As discussed above, there are specific limitations about what gases can be used in a TPC. Recent further advances in an additional gain step, the GEM (Gas Electron Multiplier), have meant that pure gases such as He can be used. GEMs operate in a similar way to Micromegas with a well-contained large electric field which generates a high gas gain through a hole drilled through a dielectric material. By stacking several gas gain stages together, a new form of GEMs was developed, known as the Multi-layer Thick GEM (M-THGEM) [33]. This modification means that the avalanche stage takes place well within the hole in the material such that secondary photons cannot propagate throughout the detector and cause sustained breakdown.

These developments are extremely important for the accessibility of α-cluster signatures which require high sensitivity when operating in active target mode — the removal of a quenching gas means that the background contaminating events are suppressed by several orders of magnitude which is an absolute necessity.

7.2 Improved position resolution

Another key component to improve the accessibility of cluster signatures in key areas is the ability to resolve tracks with high fidelity. This can be both: a) improving the angular/position resolution of tracks measured in the TPC and b) the separation of tracks from high-multiplicity events. There are three components to this position resolution: pad size, gas gain, and intrinsic pad resolution. The first of these is fairly simple, if a TPC has smaller pads, the position resolution will improve. However, the second component to this is that if the pads become smaller and smaller then for a given gas pressure, the energy loss of the particles for a single pad will decrease and correspondingly the signal amplitude and resolution will suffer and may be below threshold. Configurations with smaller pads therefore will require a higher overall gas gain. When dealing across the entire detector, this larger global gain may start to cause complications where the gas detector is approaching the Raether limit [34], effectively creating a lower limit for the pad size. Additionally, the number of electronics channels (and therefore cost and data rate) will increase with a larger number of pads.

The third component is the intrinsic pad resolution. For some detector pad sizes, the drift electrons have insufficient spread to be dispersed across multiple pads (where the electron cloud will have a Gaussian dispersion with a typical spread after drifting through a height, h, given as $\sigma \propto \sqrt{h}$) and therefore the charge measured from a single point is typically contained in one or two pixels. New detector technologies deliberately spread the charge across a series of pads giving a position resolution far below that of the pad size. Two related techniques to achieve this are currently available; the DLC (Diamond-Like Carbon) resistive layer Micromegas coating and the resistive + capacitive sharing Micromegas.

7.2.1 DLC Resistive Layer

Given that the use of a DLC Micromegas will be used for TeBAT, it will briefly be discussed here. In Fig. 9, how the incident charge from the Micromegas is incident upon a PCB with several layers is shown. The charge impinges onto the DLC coating and the charge disperses across a 2D RC network [35]. This charge spreads spatially and in a finite time which induces, via capacitive coupling, a signal on the position sensitive pads. The largest (and least delayed) signal is induced directly above where the primary electron cloud is incident on the DLC with adjacent pads having a smaller amplitude and slightly delayed signal depending on the RC value of the DLC+PCB configuration. The typical sheet resistance of the DLC used for these means it is in the range of $0.1 \div 10$ MΩ/□ (also denoted as MΩ/sq to differentiate bulk vs sheet resistance). A larger resistance also has the advantage of providing spark protection to the electronics although the spark resilience at or below a value of 1 MΩ/□ is expected to weaken. By choosing the correct DLC bulk resistance in tandem with the associated PCB capacitance, the RC value can be sensibly chosen such that the charge is dispersed across several pads with a reasonable amplitude. If the RC value is too large however, the signal produced will have a tail at long times that will significantly limit the rate capabilities of a TPC due to significant pile-up.

Simulations performed for TeBAT have shown that dispersing the charge across 4 pads either side of the primary electrons can produce a position resolution as low as 200 μm from a pad size of 3 x 3 mm^2 in ideal circumstances, far exceeding the $1/\sqrt{12}$ rule of thumb. The practical limit for the position resolution is however dependent on the gain, energy deposition of the particle and noise present in the system but resistive layer Micromegas offer an excellent opportunity to significantly improve the position resolution without drastically reducing the pad size.

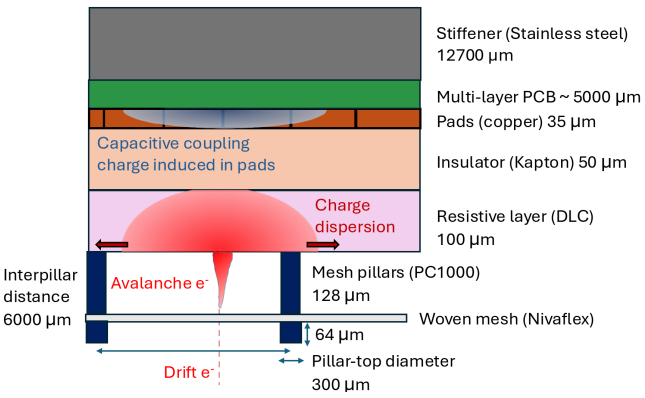

Figure 9. Schematic (not to scale) showing the composition of the DLC resistive layer Micromegas. After the drift electrons pass into the high voltage region between the DLC and woven mesh, the number of electrons drastically increases due to an avalanche. The incident charge is then spread out through the DLC which causes a signal to be induced across multiple pads due to capacitive coupling. The DLC itself is held at ground.

7.3 Overcoming beam rate limitations

One final experimental hurdle to overcome to provide a step change in cluster physics studies with TPCs is to produce a set-up that is able to take beam rates in excess of 10^6 pps. As the beam rate (energy and ion dependent) exceeds values around 10^5 pps, the space charge that is produced by the beam has an equilibrium value that is sufficient to significantly affect the electric drift field inside the TPC. This means that the tracks are perceived as being curved when reconstructed and also receive significant perturbation to the charge amplitude measured [36].

Secondly, when dealing with a TPC with a higher gain (necessary to measure low dE/dx particles such as protons) a high beam rate means that the Micromegas may struggle to recover between beam pulses and subsequently may either undergo constant breakdown damage or fail to generate an avalanche signal. Trivial solutions to this problem have included ignoring certain pads in the TPC, modifying the bias across the detector such that the beam only enters low gain portions, suppressing the drift electrons in the beam region, increasing the drift field strength and remapping the electric field map to correct for space charge aberrations. Unfortunately all these solutions do not fully solve both of the listed issues. Further development is necessary to properly address this issue such as producing a field cage that sits around the beam region to regulate the electric field in the surrounding regions and more effectively remove space charges.

The final beam rate limitation concerns the total data throughput generated with a high trigger rate and large number of channels. The TeBAT TPC has a grid of 84 x 84 pads for a total of 7056. With each channel having 12 bits of data for 512 time buckets, if every channel fires (or is set to be read out) then a single event can generate 5 MB of data. With beam rates exceeding 10^6 pps, significant electronics developments are required to be able to write ever increasing data streams without considerable dead time. Opportunities in streaming electronics such as the SALSA chip may provide such an option [37].

As radioactive beam facilities further improve their capabilities (as well as a myriad of studies possible with stable beams), inventive solutions are needed to ensure TPCs can utilise the maximum beam intensity available.

8 Conclusion

A summary of the opportunities to use TPCs to study α-cluster phenomena has been given with an emphasis on the difficulties and pitfalls one must negotiate when measuring experimental observables to compare to theory.

The need and importance of robust theoretical predictions such as the direct-decay branching ratio of the Hoyle state if it is an α-condensate is also highlighted.

The next generation of TPCs are overcoming specific limitations that limit the sensitivity of measuring α-clustering phenomena and with the advent of these devices, such as TeBAT, a new range of experiments become possible.

References

[1] A. Tohsaki, H. Horiuchi, P. Schuck, G. Röpke, Alpha cluster condensation in ^{12}c and ^{16}o, Phys. Rev. Lett. **87**, 192501 (2001). 10.1103/PhysRevLett.87.192501

[2] H. Morinaga, Interpretation of some of the excited states of $4n$ self-conjugate nuclei, Phys. Rev. **101**, 254 (1956). 10.1103/PhysRev.101.254

[3] B. Gaul, Affirming the Consequent (John Wiley & Sons, Ltd, 2018), chap. 2, pp. 42–45, ISBN 9781119165811, https://onlinelibrary.wiley.com/doi/abs/10.1002/9781119165811.ch2

[4] Y. Giomataris, P. Rebourgeard, J. Robert, G. Charpak, Micromegas: a high-granularity position-sensitive gaseous detector for high particle-flux environments, Nuclear Instruments and Methods in Physics Research Section A: Accelerators, Spectrometers, Detectors and Associated Equipment **376**, 29 (1996). https://doi.org/10.1016/0168-9002(96)00175-1

[5] M. Cortesi, J. Yurkon, A. Stolz, Operation of a thgem-based detector in low-pressure helium, Journal of Instrumentation **10**, P02012 (2015). 10.1088/1748-0221/10/02/P02012

[6] E. Koshchiy, G. Rogachev, E. Pollacco, S. Ahn, E. Uberseder, J. Hooker, J. Bishop, E. Aboud, M. Barbui, V. Goldberg et al., Texas active target (texat) detector for experiments with rare isotope beams, Nuclear Instruments and Methods in Physics Research Section A: Accelerators, Spectrometers, Detectors and Associated Equipment **957**, 163398 (2020). https://doi.org/10.1016/j.nima.2020.163398

[7] E. Epelbaum, H. Krebs, T.A. Lähde, D. Lee, U.G. Meißner, Structure and rotations of the hoyle state, Phys. Rev. Lett. **109**, 252501 (2012). 10.1103/PhysRevLett.109.252501

[8] D.J. Marín-Lámbarri, R. Bijker, M. Freer, M. Gai, Tz. Kokalova, D.J. Parker, C. Wheldon, Evidence for triangular D_{3h} symmetry in ^{12}C, Phys. Rev. Lett. **113**, 012502 (2014). 10.1103/PhysRevLett.113.012502

[9] D.N.F. Dunbar, R.E. Pixley, W.A. Wenzel, W. Whaling, The 7.68-mev state in c^{12}, Phys. Rev. **92**, 649 (1953). 10.1103/PhysRev.92.649

[10] Tz. Kokalova, N. Itagaki, W. von Oertzen, C. Wheldon, Signatures for multi-α-condensed states, Phys. Rev. Lett. **96**, 192502 (2006). 10.1103/PhysRevLett.96.192502

[11] J. Refsgaard, H. Fynbo, O. Kirsebom, K. Riisager, Three-body effects in the hoyle-state decay, Physics Letters B **779**, 414 (2018). https://doi.org/10.1016/j.physletb.2018.02.031

[12] R. Smith, J. Bishop, J. Hirst, Tz. Kokalova, C. Wheldon, The hoyle family: The search for alpha-condensate states in light nuclei, Few-Body Systems **61**, 14 (2020). 10.1007/s00601-020-1545-5

[13] J. Manfredi, R.J. Charity, K. Mercurio, R. Shane, L.G. Sobotka, A.H. Wuosmaa, A. Banu, L. Trache, R.E. Tribble, α decay of the excited states in ^{12}c at

7.65 and 9.64 mev, Phys. Rev. C **85**, 037603 (2012). 10.1103/PhysRevC.85.037603

[14] O.S. Kirsebom, M. Alcorta, M.J.G. Borge, M. Cubero, C.A. Diget, L.M. Fraile, B.R. Fulton, H.O.U. Fynbo, D. Galaviz, B. Jonson et al., Improved limit on direct α decay of the hoyle state, Phys. Rev. Lett. **108**, 202501 (2012). 10.1103/PhysRevLett.108.202501

[15] R. Smith, Tz. Kokalova, C. Wheldon, J.E. Bishop, M. Freer, N. Curtis, D.J. Parker, New measurement of the direct 3α decay from the ^{12}C hoyle state, Phys. Rev. Lett. **119**, 132502 (2017). 10.1103/PhysRevLett.119.132502

[16] D. Dell'Aquila, I. Lombardo, G. Verde, M. Vigilante, L. Acosta, C. Agodi, F. Cappuzzello, D. Carbone, M. Cavallaro, S. Cherubini et al., High-precision probe of the fully sequential decay width of the hoyle state in ^{12}C, Phys. Rev. Lett. **119**, 132501 (2017). 10.1103/PhysRevLett.119.132501

[17] T. Rana, S. Bhattacharya, C. Bhattacharya, S. Manna, S. Kundu, K. Banerjee, R. Pandey, P. Roy, A. Dhal, G. Mukherjee et al., New high precision study on the decay width of the hoyle state in 12c, Physics Letters B **793**, 130 (2019). https://doi.org/10.1016/j.physletb.2019.04.028

[18] A. Raduta, B. Borderie, E. Geraci, N. Le Neindre, P. Napolitani, M. Rivet, R. Alba, F. Amorini, G. Cardella, M. Chatterjee et al., Evidence for α-particle condensation in nuclei from the hoyle state deexcitation, Physics Letters B **705**, 65 (2011). https://doi.org/10.1016/j.physletb.2011.10.008

[19] J. Bishop, G.V. Rogachev, S. Ahn, E. Aboud, M. Barbui, A. Bosh, C. Hunt, H. Jayatissa, E. Koshchiy, R. Malecek et al., Almost medium-free measurement of the hoyle state direct-decay component with a tpc, Phys. Rev. C **102**, 041303 (2020). 10.1103/PhysRevC.102.041303

[20] R. Smith, M. Gai, M.W. Ahmed, M. Freer, H.O.U. Fynbo, D. Schweitzer, S.R. Stern, Stringent upper limit on the direct 3α decay of the hoyle state in ^{12}C, Phys. Rev. C **101**, 021302 (2020). 10.1103/PhysRevC.101.021302

[21] V.N. Efimov, Weakly bound states of three resonantly interacting particles., Yadern. Fiz. **12** (1970).

[22] P. Naidon, S. Endo, Efimov physics: a review, Reports on Progress in Physics **80**, 056001 (2017). 10.1088/1361-6633/aa50e8

[23] H. Zheng, A. Bonasera, The thomas theorem and the efimov states within a generalized bohr model, Journal of Physics Communications **4**, 085011 (2020). 10.1088/2399-6528/abaca4

[24] J. Bishop, G.V. Rogachev, S. Ahn, E. Aboud, M. Barbui, A. Bosh, J. Hooker, C. Hunt, H. Jayatissa, E. Koshchiy et al., Evidence against the efimov effect in ^{12}C from spectroscopy and astrophysics, Phys. Rev. C **103**, L051303 (2021). 10.1103/PhysRevC.103.L051303

[25] M. Munch, M. Alcorta, H.O.U. Fynbo, M. Albers, S. Almaraz-Calderon, M.L. Avila, A.D. Ayangeakaa, B.B. Back, P.F. Bertone, P.F.F. Carnelli et al., Independent measurement of the hoyle state β feeding from ^{12}B using gammasphere, Phys. Rev. C **93**, 065803 (2016). 10.1103/PhysRevC.93.065803

[26] G. Cardella, A. Bonasera, N. Martorana, L. Acosta, E. De Filippo, E. Geraci, B. Gnoffo, C. Guazzoni, L. Lo Monaco, C. Maiolino et al., Search for rare 3-α decays in the region of the hoyle state of 12c, Nuclear Physics A **1020**, 122395 (2022). https://doi.org/10.1016/j.nuclphysa.2022.122395

[27] K.P. Artemov, O.P. Belyanin, A.L. Vetoshkin, R. Wolski, M.S. Golovkov, V.Z. Goldberg, M. Madeja, V.V. Pankratov, I.N. Serikov, V.A. Timofeev et al., Effective method of study of α-cluster states, Sov. J. Nucl. Phys. USSR **52**, 408 (1990).

[28] J. Bishop, G.V. Rogachev, S. Ahn, M. Barbui, S.M. Cha, E. Harris, C. Hunt, C.H. Kim, D. Kim, S.H. Kim et al., First observation of the $\beta 3\alpha p$ decay of ^{13}O via β-delayed charged-particle spectroscopy, Phys. Rev. Lett. **130**, 222501 (2023). 10.1103/PhysRevLett.130.222501

[29] J. Bishop, G.V. Rogachev, S. Ahn, M. Barbui, S.M. Cha, E. Harris, C. Hunt, C.H. Kim, D. Kim, S.H. Kim et al., Cluster structure of $3\alpha + p$ states in ^{13}N, Phys. Rev. C **109**, 054308 (2024). 10.1103/PhysRevC.109.054308

[30] C. Wheldon, T. Kokalova, M. Freer, J. Walshe, R. Hertenberger, H.F. Wirth, N.I. Ashwood, M. Barr, N. Curtis, T. Faestermann et al., Spectroscopy of ^{9}B via high-resolution ejectile-tagged recoil breakup, Phys. Rev. C **91**, 024308 (2015). 10.1103/PhysRevC.91.024308

[31] H. Fortune, R. Sherr, Update on b9(1/2+), Nuclear Physics A **898**, 78 (2013). https://doi.org/10.1016/j.nuclphysa.2012.12.120

[32] H.H. Knudsen, H.O.U. Fynbo, M.J.G. Borge, R. Boutami, P. Dendooven, C.A. Diget, T. Eronen, S. Fox, L.M. Fraile, B. Fulton et al., β-decay of ^{13}O, Phys. Rev. C **72**, 044312 (2005). 10.1103/PhysRevC.72.044312

[33] M. Cortesi, S. Rost, W. Mittig, Y. Ayyad-Limonge, D. Bazin, J. Yurkon, A. Stolz, Multi-layer thick gas electron multiplier (M-THGEM): A new MPGD structure for high-gain operation at low-pressure, Review of Scientific Instruments **88**, 013303 (2017), https://pubs.aip.org/aip/rsi/article-pdf/doi/10.106 10.1063/1.4974333

[34] P. Fonte, V. Peskov, F. Sauli, Feedback and breakdown in parallel-plate chambers, Nuclear Instruments and Methods in Physics Research Section A: Accelerators, Spectrometers, Detectors and Associated Equipment **305**, 91 (1991). https://doi.org/10.1016/0168-9002(91)90522-R

[35] M. Dixit, A. Rankin, Simulating the charge dispersion phenomena in micro pattern gas detectors with a resistive anode, Nuclear Instruments and Methods in Physics Research Section A: Accelerators, Spectrometers, Detectors

and Associated Equipment **566**, 281 (2006). https://doi.org/10.1016/j.nima.2006.06.050

[36] J. Randhawa, M. Cortesi, Y. Ayyad, W. Mittig, T. Ahn, D. Bazin, S. Beceiro-Novo, L. Carpenter, K. Cook, M. Dasgupta et al., Beam-induced space-charge effects in time projection chambers in low-energy nuclear physics experiments, Nuclear Instruments and Methods in Physics Research Section A: Accelerators, Spectrometers, Detectors and Associated Equipment **948**, 162830 (2019). https://doi.org/10.1016/j.nima.2019.162830

[37] D. Neyret, Salsa: a new versatile readout chip for mpgd, https://indico.cern.ch/event/1413681/contributions/5998174/attachments/2880954/5047202/SALSA_DRD1_Electronics_workshop_20240619.pdf